Supporting Information

Mg-doped layered vanadate for high-energy zinc anode-based electrochromic devices

Haoyang Dong[a], Mengjie Zhu[a], Caofeng Niu[a], Guolong Zhou[a], Tongzhuang He[a], Bing Xu[a, *], Jingwei Chen[a, b, *]

[a]School of Materials Science and Engineering, Ocean University of China, Qingdao 266100, China.

[b]Qingdao Key Laboratory of Marine Extreme Environment Materials, Qingdao 266404, China.

E-mail: bxu0117@163.com; chenjingwei@ouc.edu.cn

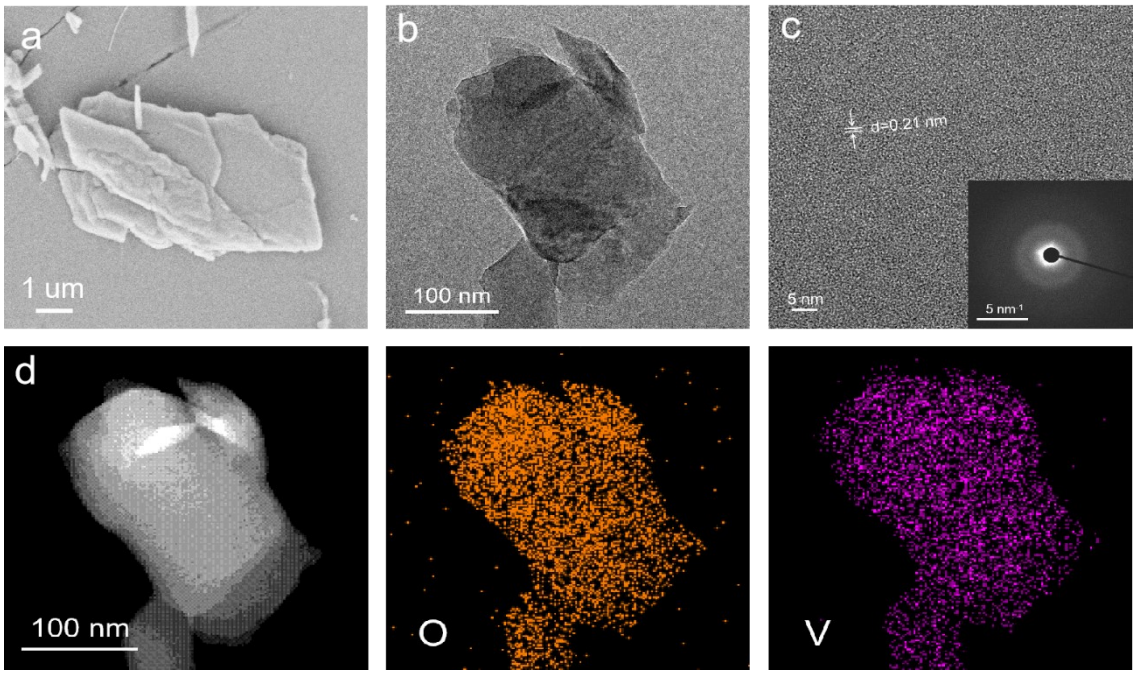

Fig. S1 Electron microscope observations of VO. (a) SEM images of VO. (b) TEM images of VO. (c) High-resolution images of VO (HRTEM). (d) HAADF-STEM images of VO and corresponding element mappings.

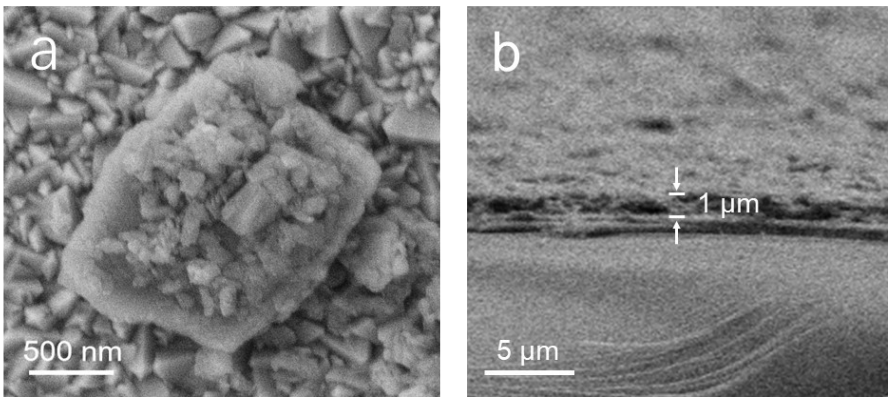

Fig. S2 (a) SEM image of MVO. (b) Cross-sectional SEM image of MVO.

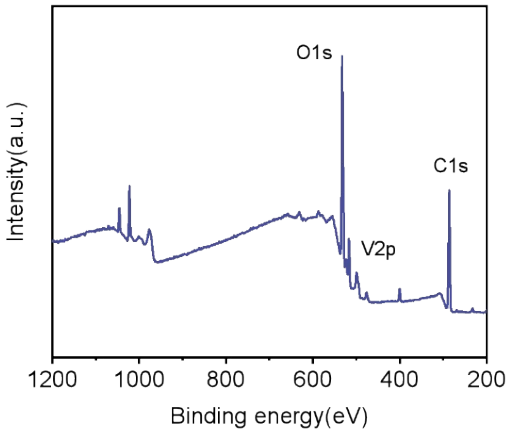

Fig. S3 XPS full-survey spectrum of MVO.

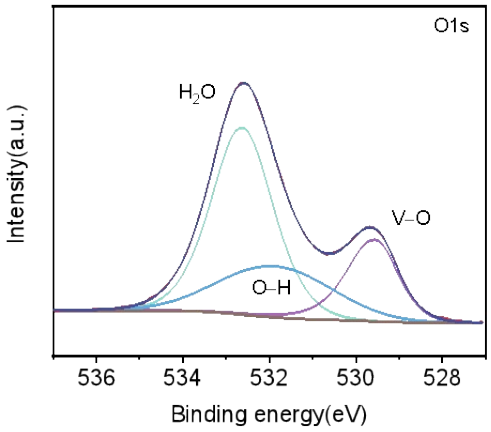

Fig. S4 High-resolution O 1s XPS spectra of MVO.

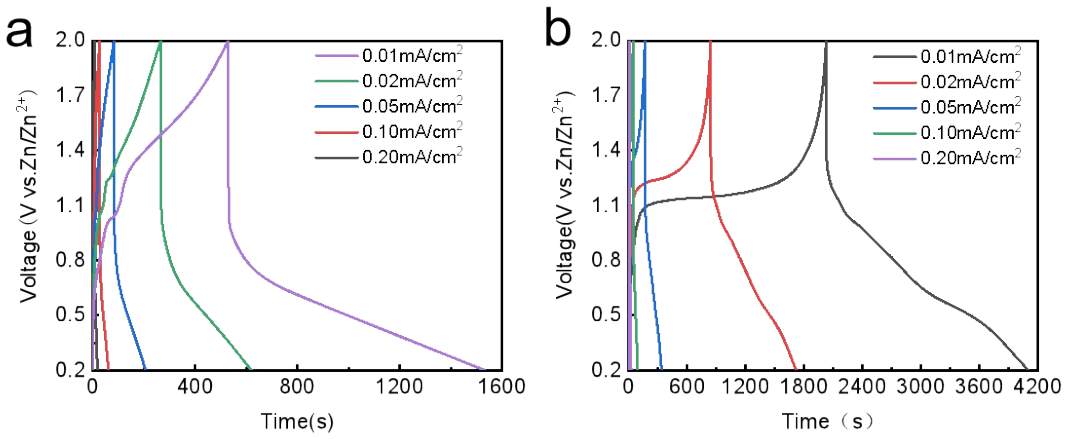

Fig. S5 a) GCD curves of VO at different current densities. b) GCD curves of MVO at different current densities.

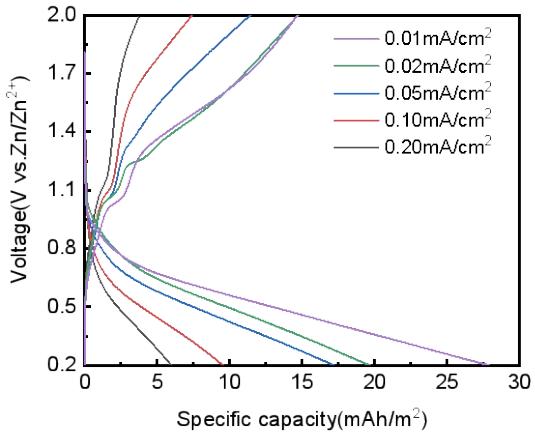

Fig. S6 GCD curves of VO quantified at different current densities.

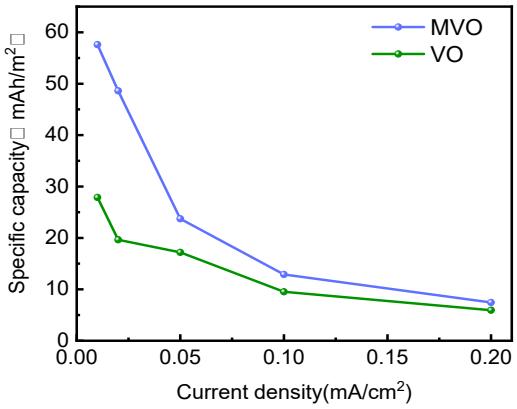

Fig. S7 Specific capacities of VO and MVO at different current densities.

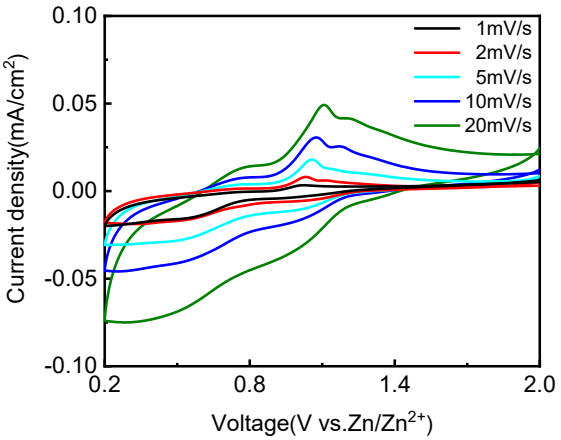

Fig. S8 CV curves of VO at different scanning rates.

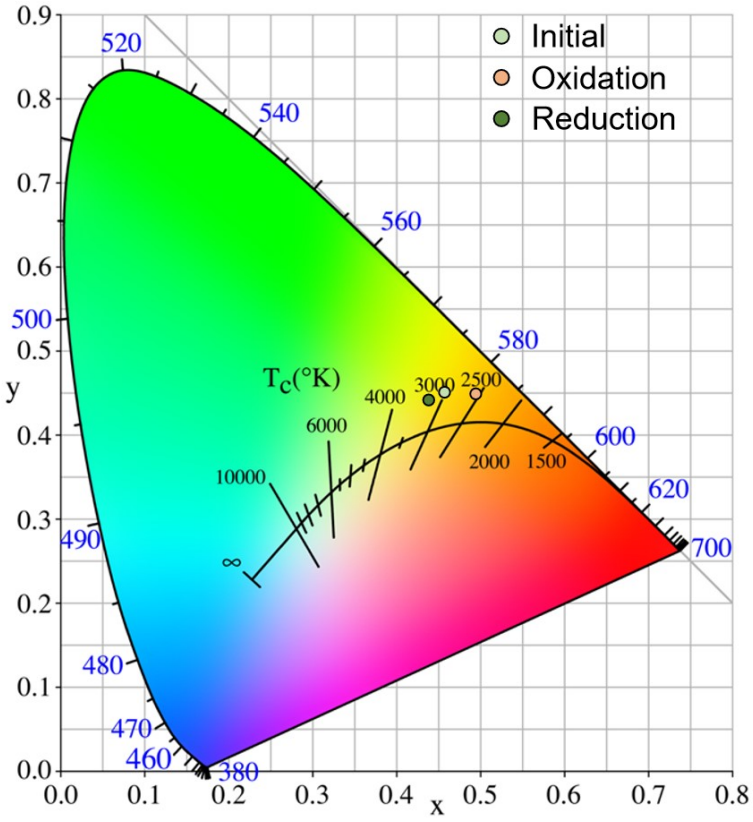

Fig. S9 The CIE1931 chromaticity chart of MVO.

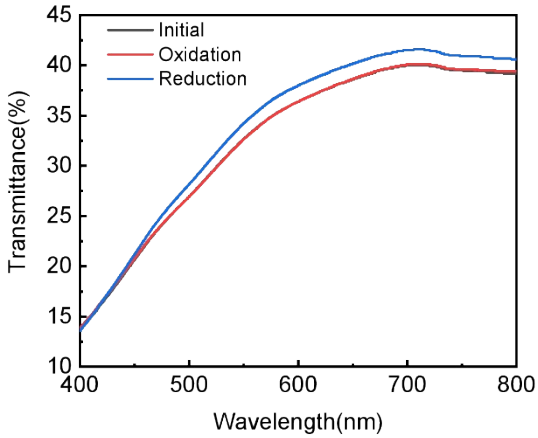

Fig. S10 Transmittance spectra of the initial state, oxidation state and reduction state of VO at 400-800 nm.

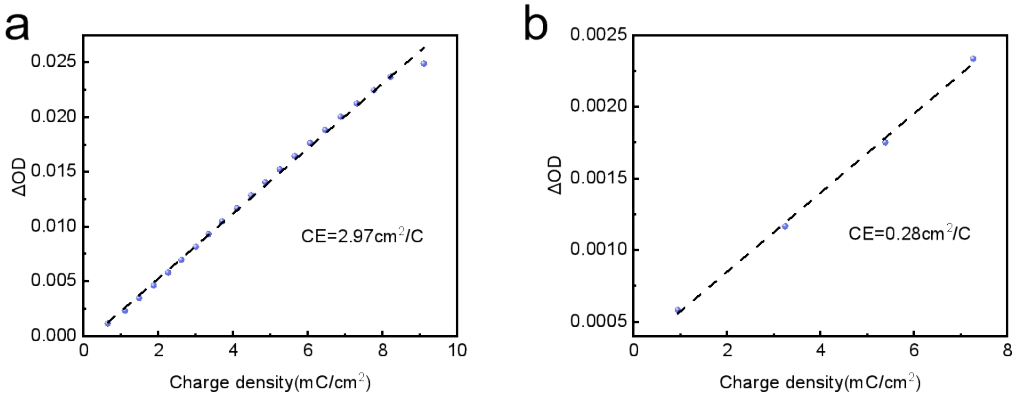

Fig. S11 Relationship between in-situ optical density and charge density of MVO a) and VO b) at 650 nm during the coloring process.

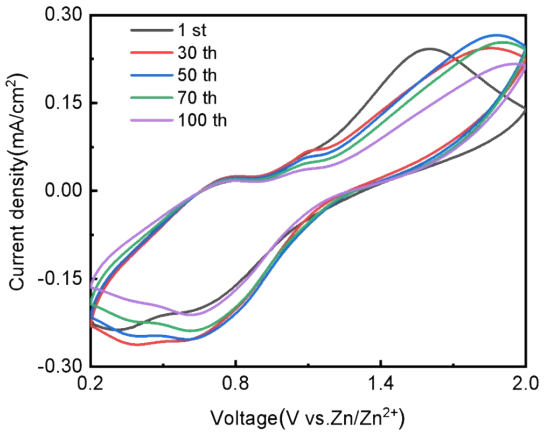

Fig. S12 The CV curves of MVO for 100 cycles at a scan rate of 50 mV s^{-1} within 0.2-2 V.

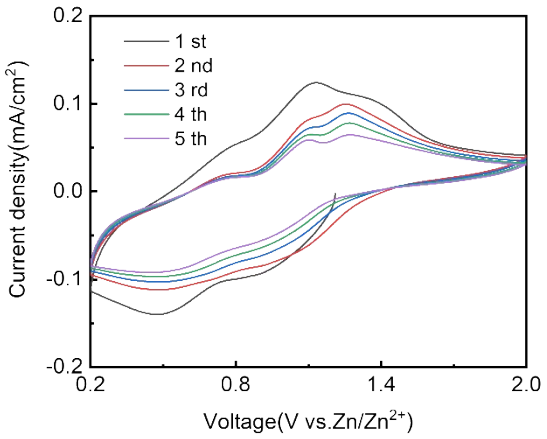

Fig. S13 The CV curves of the VO electrochromic device in the first five cycles at 20 mV s^{-1}.

Table S1. Optical measurement data of MVO and VO

Produced Film	$t_{colored}$ (s)	$t_{bleached}$ (s)	$T_{colored}$ (%)	$T_{bleached}$ (%)	CE (cm^2/C)
VO	91.2	42	37.1	37.3	0.28
MVO	79.6	25.2	35.6	37.7	2.97